Optical properties of $BaMnF_4$

T. Asahi, M. Tomizawa, and J. Kobayashi
Department of Applied Physics, Waseda University, 3-4-1 Ohkubo, Shinjuku-ku, Tokyo 169, Japan

W. Kleemann
Angewandte Physik, Universität Duisburg, W-4100 Duisburg, Germany
(Received 9 July 1991)

Optical properties of pyroelectric and antiferromagnetic $BaMnF_4$ were studied by using a high-accuracy universal polarimeter in the temperature range including the incommensurate phase transition point T_i. Both phases above and below T_i were found to be optically active. The active gyration tensor components g_{ij} were consistent with the reported symmetry of the crystal, i.e., C_{2v} and C_2 above and below T_i. Temperature dependences of all the gyration components were measured. It is striking that g_{23}, which exists commonly in both phases, manifested itself a sharp peak at T_i. This divergence of g_{23} makes the transition perfectly second order. g_{11} along the incommensurate a axis develops conspicuously. The present results of the birefringences did not perfectly agree with previous reports: Although the temperature dependence of Δn_c coincided with the result of Schäfer *et al.*, those of Δn_a and Δn_b were quite different in their report. Rotation of the indicatrix takes place only around the a axis of the low-temperature phase. This fact confirms the validity of the point group C_2 of the low-temperature phase. The rotation angle of the indicatrix was found to be one order of magnitude larger than that of the crystallographic axes. The rotation angle of the gyration surface was also evaluated. It is approximately two orders of magnitude larger than the rotation angle of the indicatrix. This fact clearly indicates that gyrations are very sensitively affected by the change of the order parameter.

I. INTRODUCTION

$BaMnF_4$ is attracting much interest since it exhibits peculiar pyroelectric and antiferromagnetic phases.[1,2] In particular, an incommensurate (abbreviated as IC henceforth) modulation takes place below a structural transition point T_i of 250 K, keeping the pyroelectric state from the high-temperature side.[3] The high-temperature phase (HTP) above T_i belongs to an orthorhombic space group, C_{2v}^{12} ($A2_1am$).[4] The IC modulation in the low-temperature phase (LTP) below T_i occurs along the a axis with a wave vector $\mathbf{q}=(0.39, 0.5, 0.5)$, accompanying doubling of the unit cell in the (100) plane. The physical character of the IC modulation of $BaMnF_4$ seems essentially different from that of modulations occurred in A_2BX_4 type ferroelectrics on which a considerable number of studies were made.[5] For instance, the length of the modulation wave vector of $BaMnF_4$ hardly depends on temperature, and the IC phase does not transform into a commensurate phase through a lock-in transition.[3,6,7]

Cox *et al.*[3,6] proposed two alternative models for the IC structure, which were consistent with the theoretical predictions offered by Dvořák and Fousek[8]: One model realizes an average structure of LTP with the same symmetry as HTP, while another model an average structure of LTP with a reduced symmetry to the monoclinic system. In reality, the symmetry of the average structure of LTP was successfully determined as C_2 by Ryan[9] by using x rays, and that was confirmed by St.-Grégoire *et al.*[10] and Ogawa *et al.*[11]

On the other hand, considerable data were accumulated of optical properties of this crystal. Eibschütz and Guggenheim[1] determined the refractive indices at room temperature, i.e., $n_a=1.499$, $n_b=1.480$, and $n_c=1.505$, at the wavelength of 5893 Å. Birefringences were measured by three groups.[12–14] Régis *et al.*[12] revealed the temperature dependence of Δn_b, birefringence along the b axis, by using a Babinet-Soleil compensator. Pisarev *et al.*[13] used both interferometric and polarimetric methods and measured the temperature change of the refractive indices and birefringences. They drew attention to measure a rotation angle of the indicatrix, and further optical gyration in LTP. Schäfer *et al.*[14] used an elaborate modulation technique for birefringence measurements with a resolution of 10^{-8} for 1-mm-thick crystals. The results of Régis *et al.* and of Schäfer *et al.* were fairly agreed, and they have been confirmed recently by St.-Grégoire *et al.*[15]

Judging from the consistency between the results in the papers of Régis's and Schäfer's groups, their results seemed to be correct beyond any doubt. However, their results were not perfectly convincing on the following two points: the birefringences in HTP decreased with decreasing temperature, and the measurements in LTP were performed with a complete neglect of possible rotations of the indicatrix. Thus we felt it necessary to make an optical study on both phases of $BaMnF_4$ with proper allowance for the rotation of the indicatrix and optical gyration. In particular, the knowledge of the optical activity is needed for the elucidation of the IC phase transitions, as have recently been illustrated by us,[16–19] with regard to the A_2BX_4 family. It becomes possible to mea-

sure birefringences, gyrations, and rotations of the indicatrix of any crystals simultaneously by using a HAUP,[16,20,21] high accuracy universal polarimeter. However optical study of this crystal is extremely difficult, since the LTP is monoclinic. We already applied HAUP method to this crystal.[22,23] However, the recent crucial reexamination still disclosed that the previous reports contained errors in gyrations and rotations of the indicatrix along the crystallographic b and c axes.[22] This paper reports the revised results of our comprehensive optical study of $BaMnF_4$ by using the improved HAUP method.

II. PHENOMENOLOGICAL RELATIONS OF OPTICAL PROPERTIES

First, we solve the phenomenological theories for change of birefringences, gyrations, and rotations of indicatrix, which will occur when the crystal changes from HTP to LTP. The point group of HTP is known to be C_{2v}.[4] On the other hand, the true symmetry of LTP cannot be represented by a three-dimensional space group,[24] as the IC modulation takes place in it.[3,6,7] Recently it was revealed[19] that optical activity sensitively reflects the incommensurability of crystal structure. Considering these circumstances we took the following scheme of analysis: We preliminarily assumed that all the components of the gyration tensor were present in LTP and tried to eliminate the inactive components by the experiments. However, as far as the birefringences were concerned we regarded it sufficiently valid to identify LTP as C_2,[9,10,11,25] since they were not sensitive to the chirality of the structure.

The lattice constants of HTP were reported as $a=5.984\pm3$ Å, $b=15.098\pm2$ Å, and $c=4.2216\pm3$ Å at room temperature.[4] We confirmed these values by using x rays and identified the three crystallographic axes with the principal axes of the indicatrix, say, x_1, x_2, and x_3 axes, respectively.

Define the components of the dielectric impermeability and gyration tensors as B_{ij} and g_{ij} $(i,j=1,2,3)$, and the rotation angles of the indicatrix as ψ_k or ψ_{kl} $(k,l=a,b,c)$. The components B_{ij} and g_{ij} of the two phases are represented in Fig. 1 by the matrix form referring to the (x_1,x_2,x_3) axes.

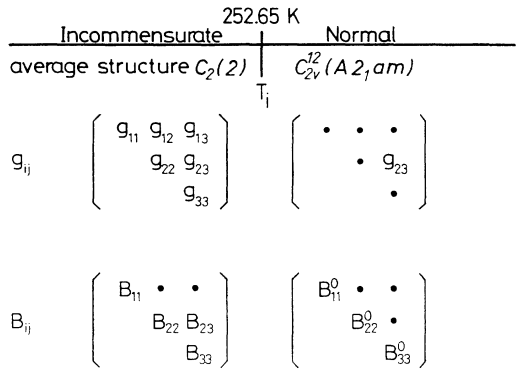

FIG. 1. Gyration tensors g_{ij} and dielectric impermeability tensors B_{ij} of $BaMnF_4$ together with phase diagram.

HAUP measurements were performed on the following six different cases: They are classified by the direction of the wave vector **s** of the incident light with respect to (x_1,x_2,x_3) axes in the crystal.

(A) Case-1; **s** was parallel to the x_1 axis. (B) Case-2; **s** parallel to the x_2 axis. (C) Case-3; **s** parallel to the x_3 axis. (D) Case-4; **s** parallel to the direction which was contained in (001) plane and made 45° with the x_1 axis. (E) Case-5; **s** parallel to the direction in (010) plane making 45° with the x_3 axis. (F) Case-6; **s** parallel to the direction in (100) plane making 45° with the x_2 axis.

Phenomenological treatments will be done in these six cases.

A. Case-1

The equation of the indicatrix of HTP is written by using B_{ij}^0 components indicated in Fig. 1:

$$B_{11}^0x_1^2+B_{22}^0x_2^2+B_{33}^0x_3^2=1\ , \tag{1}$$

where $B_{11}^0=1/n_1^{02}$, $B_{22}^0=1/n_2^{02}$, and $B_{33}^0=1/n_3^{02}$. The intersection ellipse between a plane through the origin that is normal to **s** and the indicatrix (1) is given by substituting $x_1=0$ to (1),

$$B_{22}^0x_2^2+B_{33}^0x_3^2=1\ . \tag{2}$$

The birefringence observed in this case, Δn_a^0, is derived:

$$\Delta n_a^0=\frac{1}{\sqrt{B_{33}^0}}-\frac{1}{\sqrt{B_{22}^0}}=n_3^0-n_2^0\ . \tag{3}$$

The indicatrix of LTP is expressed by using B_{ij} components:

$$B_{11}x_1^2+B_{22}x_2^2+B_{33}x_3^2+2B_{23}x_2x_3=1\ . \tag{4}$$

The corresponding intersection ellipse is expressed as

$$B_{22}x_2^2+B_{33}x_3^2+2B_{23}x_2x_3=1\ , \tag{5}$$

where $B_{11}=B_{11}^0+\delta B_{11}$, $B_{22}=B_{22}^0+\delta B_{22}$, and $B_{33}=B_{33}^0+\delta B_{33}$. The equation indicates that the principal axes are rotated from the old principal axes around the x_1 axis. Here let us define the new principal axes of the ellipse as (x_2',x_3'), and the tensor components referred to them as B_{22}' and B_{33}'. Then the equation changes to

$$B_{22}'x_2'^2+B_{33}'x_3'^2=1\ . \tag{6}$$

The relation among the new and old components and the rotation angle ψ_a of the indicatrix around the x_1 axis can be solved by the Mohr circle construction[26]

$$B_{22}'=\tfrac{1}{2}(B_{22}+B_{33})+r'\ , \tag{7a}$$

$$B_{33}'=\tfrac{1}{2}(B_{22}+B_{33})-r'\ , \tag{7b}$$

and

$$\tan(2\psi_a)=\frac{2B_{23}}{B_{33}-B_{22}}\ , \tag{7c}$$

where

$$r'=[\tfrac{1}{4}(B_{22}-B_{33})^2+B_{23}^2]^{1/2} . \tag{7d}$$

Judging from the x-ray evidence that the monoclinic angle was as small as 0.02° at 240K,[9-11] ψ_a will also be so small that r' can be expressed in a good approximation by

$$r'\simeq\frac{1}{2}(B_{22}-B_{33})+\frac{B_{23}^2}{B_{22}-B_{33}} . \tag{7e}$$

Thus

$$B'_{22}\simeq B_{22}+\frac{B_{23}^2}{B_{22}-B_{33}} \tag{8a}$$

and

$$B'_{33}\simeq B_{33}-\frac{B_{23}^2}{B_{22}-B_{33}} . \tag{8b}$$

The birefringence Δn_a and the rotation angle ψ_a can be deduced as

$$\Delta n_a=\frac{1}{\sqrt{B'_{33}}}-\frac{1}{\sqrt{B'_{22}}}=B_{33}^{-1/2}\left[1-\frac{B_{23}^2}{B_{33}(B_{22}-B_{33})}\right]^{-1/2}-B_{22}^{-1/2}\left[1+\frac{B_{23}^2}{B_{22}(B_{22}-B_{33})}\right]^{-1/2}$$
$$\simeq n_3^0-n_2^0+\frac{1}{2}\left[(n_2^{03}\delta B_{22}-n_3^{03}\delta B_{33})+\frac{(n_3^{03}+n_2^{03})B_{23}^2}{(1/n_2^0)^2-(1/n_3^0)^2}\right] \tag{9}$$

and

$$\psi_a\simeq\frac{B_{23}}{B_{33}^0-B_{22}^0}=\frac{B_{23}}{(1/n_3^0)^2-(1/n_2^0)^2}$$
$$=\frac{n_2^{02}n_3^{02}B_{23}}{(n_2^{02}-n_3^{02})} . \tag{10}$$

Define the observed gyration in this case as G_a. It can be expressed by gyration tensor components by using the direction cosines of s ($l_1=1$, $l_2=0$, $l_3=0$):

$$G_a=\sum_{i,j}g_{ij}l_il_j=g_{11} . \tag{11}$$

From the symmetry, it must be zero in HTP.

B. Case-2

The equation of the intersection ellipse of HTP is obtained by substituting $x_2=0$ into (1):

$$B_{11}^0x_1^2+B_{33}^0x_3^2=1 . \tag{12}$$

Therefore

$$\Delta n_b^0=n_3^0-n_1^0 . \tag{13}$$

The intersection ellipse of LTP is derived from (4) by putting $x_2=0$. So the birefringence is represented as

$$\Delta n_b=\frac{1}{\sqrt{B_{33}}}-\frac{1}{\sqrt{B_{11}}}$$
$$\simeq n_3^0-n_1^0+\tfrac{1}{2}(n_1^{03}\delta B_{11}-n_3^{03}\delta B_{33}) . \tag{14}$$

As the direction cosines are expressed as s (0,1,0), the gyration G_b is given as

$$G_b=g_{22} , \tag{15}$$

which is zero in HTP.

C. Case-3

The intersection ellipse of HTP is written as

$$B_{11}^0x_1^2+B_{22}^0x_2^2=1 \tag{16}$$

and

$$\Delta n_c^0=n_1^0-n_2^0 . \tag{17}$$

Birefringence of LTP can be obtained by putting $x_3=0$ into (4):

$$\Delta n_c\simeq n_1^0-n_2^0+\tfrac{1}{2}(n_2^{03}\delta B_{22}-n_1^{03}\delta B_{11}) . \tag{18}$$

The gyration of both phases is given as

$$G_c=g_{33} , \tag{19}$$

which is zero in HTP.

D. Case-4

The equation of the indicatrix in HTP must be written, at first, referring to the new coordinate axes (x_1'',x_2'',x_3''), which are obtained by rotating the original ones by 45° around the x_3 axis. Both coordinates are related by

$$\begin{bmatrix}x_1\\x_2\\x_3\end{bmatrix}=\begin{bmatrix}\cos\left[\frac{\pi}{4}\right] & \cos\left[\frac{3}{4}\pi\right] & 0\\ \cos\left[-\frac{\pi}{4}\right] & \cos\left[\frac{\pi}{4}\right] & 0\\ 0 & 0 & 1\end{bmatrix}\begin{bmatrix}x_1''\\x_2''\\x_3''\end{bmatrix}$$
$$=\begin{bmatrix}\frac{1}{\sqrt{2}}(x_1''-x_2'')\\ \frac{1}{\sqrt{2}}(x_1''+x_2'')\\ x_3''\end{bmatrix} . \tag{20}$$

By substituting this relation to (1)

$$B_{11}^{0''}x_1''^2+B_{22}^{0''}x_2''^2+B_{33}^{0''}x_3''^2+2B_{12}^{0''}x_1''x_2''=1 , \tag{21}$$

where

$$B^{0\prime\prime}_{11}=B^{0\prime\prime}_{22}=\tfrac{1}{2}(B^{0}_{11}+B^{0}_{22}) , \tag{22a}$$

$$B^{0\prime\prime}_{33}=B^{0}_{33} , \tag{22b}$$

and

$$B^{0\prime\prime}_{12}=\tfrac{1}{2}(B^{0}_{22}-B^{0}_{11}) . \tag{22c}$$

Here the equation of the intersection ellipse can be obtained by letting $x_1''=0$ in (21):

$$B^{0\prime\prime}_{22}x_2''^2+B^{0\prime\prime}_{33}x_3''^2=1 . \tag{23}$$

Then the birefringence Δn^0_{ab} in this case is derived as

$$\Delta n^0_{ab}=\frac{1}{\sqrt{B^{0\prime\prime}_{33}}}-\frac{1}{\sqrt{B^{0\prime\prime}_{22}}}=n^0_3-\frac{\sqrt{2}\,n^0_1 n^0_2}{(n^{02}_1+n^{02}_2)^{1/2}} . \tag{24}$$

In LTP the same procedure as in HTP is applied to (4),

$$B''_{11}x_1''^2+B''_{22}x_2''^2+B''_{33}x_3''^2+2B''_{23}x_2''x_3''+2B''_{31}x_3''x_1''+2B''_{12}x_1''x_2''=1 , \tag{25}$$

where

$$B''_{11}=B''_{22}=\tfrac{1}{2}(B_{11}+B_{22}) , \tag{26a}$$

$$B''_{33}=B_{33} , \tag{26b}$$

$$B''_{13}=B''_{23}=\frac{\sqrt{2}}{2}B_{23} , \tag{26c}$$

and

$$B''_{12}=\tfrac{1}{2}(B_{22}-B_{11}) . \tag{26d}$$

The equation of the intersection ellipse is obtained also by putting $x_1''=0$:

$$B''_{22}x_2''^2+B''_{33}x_3''^2+2B''_{23}x_2''x_3''=1 . \tag{27}$$

This equation is rewritten by referring to the principal coordinate axes (x_1''',x_2''',x_3'''), which are obtained by rotating the previous ones by ψ_{ab} around the x_1'' axis:

$$B'''_{22}x_2'''^2+B'''_{33}x_3'''^2=1 , \tag{28}$$

where

$$B'''_{22}=\tfrac{1}{2}(B''_{22}+B''_{33})+r''' , \tag{29a}$$

$$B'''_{33}=\tfrac{1}{2}(B''_{22}+B''_{33})-r''' , \tag{29b}$$

$$\tan(2\psi_{ab})=\frac{2B''_{23}}{B''_{33}-B''_{22}} , \tag{29c}$$

and

$$r'''=[\tfrac{1}{4}(B''_{22}-B''_{33})^2+B''^2_{23}]^{1/2} . \tag{29d}$$

By the same reason as in (7e), r''' is approximated as

$$r'''\simeq\tfrac{1}{2}(B''_{22}-B''_{33})+\frac{B''^2_{23}}{B''_{22}-B''_{33}} . \tag{29e}$$

Thus

$$B'''_{22}=B''_{22}+\frac{B''^2_{23}}{B''_{22}-B''_{33}} \tag{30a}$$

and

$$B'''_{33}=B''_{33}-\frac{B''^2_{23}}{B''_{22}-B''_{33}} . \tag{30b}$$

Then the birefringence Δn_{ab} can be obtained by using (26a), (26b), and (26c):

$$\Delta n_{ab}=\frac{1}{\sqrt{B'''_{33}}}-\frac{1}{\sqrt{B'''_{22}}}\simeq n^0_3-\frac{\sqrt{2}\,n^0_1 n^0_2}{(n^{02}_1+n^{02}_2)^{1/2}}+\frac{1}{2}\left[\frac{\sqrt{2}\,n^{03}_1 n^{03}_2}{(n^{02}_1+n^{02}_2)^{3/2}}(\delta B_{11}+\delta B_{22})-n^{03}_3\delta B_{33}\right]$$
$$+\frac{1}{2}(n^0_1 n^0_2 n^0_3 B_{23})^2\frac{\left[n^{03}_3+\dfrac{2\sqrt{2}\,n^{03}_1 n^{03}_2}{(n^{02}_1+n^{02}_2)^{3/2}}\right]}{n^{02}_2 n^{02}_3+n^{02}_1 n^{02}_3-2n^{02}_1 n^{02}_2} \tag{31}$$

and

$$\psi_{ab}\simeq\frac{\sqrt{2}(n^0_1 n^0_2 n^0_3)^2 B_{23}}{2n^{02}_1 n^{02}_2-(n^{02}_2 n^{02}_3+n^{02}_1 n^{02}_3)} . \tag{32}$$

The gyration G_{ab} is obtained by using $\mathbf{s}=(1/\sqrt{2},1/\sqrt{2},0)$,

$$G_{ab}=\tfrac{1}{2}(g_{11}+g_{22})+g_{12} , \tag{33}$$

which vanishes in HTP.

E. Case-5

The equation of the indicatrix must be written referring to the new coordinate axes (x_1'',x_2'',x_3''), which are obtained by rotating the old ones by 45° around the x_2 axis. Both coordinates are related by

$$\begin{bmatrix}x_1\\x_2\\x_3\end{bmatrix}=\begin{bmatrix}\cos\left[\frac{\pi}{4}\right] & 0 & \cos\left[-\frac{\pi}{4}\right]\\ 0 & 1 & 0\\ \cos\left[\frac{3}{4}\pi\right] & 0 & \cos\left[\frac{\pi}{4}\right]\end{bmatrix}\begin{bmatrix}x_1''\\x_2''\\x_3''\end{bmatrix}$$
$$=\begin{bmatrix}\frac{1}{\sqrt{2}}(x_1''+x_3'')\\ x_2''\\ \frac{1}{\sqrt{2}}(-x_1''+x_3'')\end{bmatrix} . \tag{34}$$

By substituting (34) into (1)

$$B_{11}^{0\prime\prime}x_1^{\prime\prime 2}+B_{22}^{0\prime\prime}x_2^{\prime\prime 2}+B_{33}^{0\prime\prime}x_3^{\prime\prime 2}+2B_{31}^{0\prime\prime}x_3^{\prime\prime}x_1^{\prime\prime}=1 , \quad (35)$$

where

$$B_{11}^{0\prime\prime}=B_{33}^{0\prime\prime}=\tfrac{1}{2}(B_{11}^{0}+B_{33}^{0}) , \quad (36a)$$

$$B_{22}^{0\prime\prime}=B_{22}^{0} , \quad (36b)$$

and

$$B_{31}^{0\prime\prime}=\tfrac{1}{2}(B_{11}^{0}-B_{33}^{0}) . \quad (36c)$$

The equation of the intersection ellipse is obtained by letting $x_3^{\prime\prime}=0$ in (35):

$$B_{11}^{0\prime\prime}x_1^{\prime\prime 2}+B_{22}^{0\prime\prime}x_2^{\prime\prime 2}=1 . \quad (37)$$

Therefore

$$\Delta n_{ca}^{0}=\frac{1}{\sqrt{B_{11}^{0\prime\prime}}}-\frac{1}{\sqrt{B_{22}^{0\prime\prime}}}=\frac{\sqrt{2}\,n_1^0 n_3^0}{(n_1^{02}+n_3^{02})^{1/2}}-n_2^0 . \quad (38)$$

In LTP, the equation of the indicatrix can be obtained by substituting (34) into (4),

$$B_{11}^{\prime\prime}x_1^{\prime\prime 2}+B_{22}^{\prime\prime}x_2^{\prime\prime 2}+B_{33}^{\prime\prime}x_3^{\prime\prime 2}+2B_{23}^{\prime\prime}x_2^{\prime\prime}x_3^{\prime\prime}+2B_{31}^{\prime\prime}x_3^{\prime\prime}x_1^{\prime\prime}+2B_{12}^{\prime\prime}x_1^{\prime\prime}x_2^{\prime\prime}=1 , \quad (39)$$

where

$$B_{11}^{\prime\prime}=B_{33}^{\prime\prime}=\tfrac{1}{2}(B_{11}+B_{33}) , \quad (40a)$$

$$B_{22}^{\prime\prime}=B_{22} , \quad (40b)$$

$$B_{23}^{\prime\prime}=-B_{12}^{\prime\prime}=\frac{\sqrt{2}}{2}B_{23} , \quad (40c)$$

and

$$B_{31}^{\prime\prime}=\tfrac{1}{2}(B_{11}-B_{33}) . \quad (40d)$$

Then the equation of the intersection ellipse is written by letting $x_3^{\prime\prime}=0$:

$$B_{11}^{\prime\prime}x_1^{\prime\prime 2}+B_{22}^{\prime\prime}x_2^{\prime\prime 2}+2B_{12}^{\prime\prime}x_1^{\prime\prime}x_2^{\prime\prime}=1 . \quad (41)$$

This is expressed by the principal coordinate axes $(x_1^{\prime\prime\prime},x_2^{\prime\prime\prime},x_3^{\prime\prime\prime})$, which are rotated by ψ_{ca} around the $x_3^{\prime\prime}$ axis:

$$B_{11}^{\prime\prime\prime}x_1^{\prime\prime\prime 2}+B_{22}^{\prime\prime\prime}x_2^{\prime\prime\prime 2}=1 , \quad (42)$$

where

$$B_{11}^{\prime\prime\prime}\simeq B_{11}^{\prime\prime}-\frac{B_{12}^{\prime\prime 2}}{B_{22}^{\prime\prime}-B_{11}^{\prime\prime}} , \quad (43a)$$

$$B_{22}^{\prime\prime\prime}\simeq B_{22}^{\prime\prime}+\frac{B_{12}^{\prime\prime 2}}{B_{22}^{\prime\prime}-B_{11}^{\prime\prime}} , \quad (43b)$$

and

$$\psi_{ca}\simeq\frac{B_{12}^{\prime\prime}}{B_{22}^{\prime\prime}-B_{11}^{\prime\prime}} . \quad (43c)$$

Then

$$\Delta n_{ca}=\frac{1}{\sqrt{B_{11}^{\prime\prime\prime}}}-\frac{1}{\sqrt{B_{22}^{\prime\prime\prime}}}\simeq\frac{\sqrt{2}\,n_1^0 n_3^0}{(n_1^{02}+n_3^{02})^{1/2}}-n_2^0-\frac{1}{2}\left[\frac{\sqrt{2}\,n_1^{03}n_3^{03}}{(n_1^{02}+n_3^{02})^{3/2}}(\delta B_{11}+\delta B_{33})-n_2^{03}\delta B_{22}\right]$$
$$-\frac{1}{2}(n_1^0 n_2^0 n_3^0 B_{23})^2\frac{\left[\frac{2\sqrt{2}\,n_1^{03}n_3^{03}}{(n_1^{02}+n_3^{02})^{3/2}}+n_2^{03}\right]}{n_2^{02}n_3^{02}+n_1^{02}n_2^{02}-2n_1^{02}n_3^{02}} \quad (44)$$

and

$$\psi_{ca}\simeq\frac{\sqrt{2}(n_1^0 n_2^0 n_3^0)^2 B_{23}}{n_2^{02}n_3^{02}+n_1^{02}n_2^{02}-2n_1^{02}n_3^{02}} . \quad (45)$$

Letting $\mathbf{s}=(1/\sqrt{2},0,1/\sqrt{2})$ in both phases,

$$G_{ca}=\tfrac{1}{2}(g_{11}+g_{33})+g_{13} , \quad (46)$$

which vanishes in HTP.

F. Case-6

The relation between the old and new coordinate axes, which are rotated by 45° around x_1 axis, is given:

$$\begin{bmatrix}x_1\\x_2\\x_3\end{bmatrix}=\begin{bmatrix}x_1^{\prime\prime}\\\frac{1}{\sqrt{2}}(x_2^{\prime\prime}-x_3^{\prime\prime})\\\frac{1}{\sqrt{2}}(x_2^{\prime\prime}+x_3^{\prime\prime})\end{bmatrix} . \quad (47)$$

By substituting this relation into (1)

$$B_{11}^{0\prime\prime}x_1^{\prime\prime 2}+B_{22}^{0\prime\prime}x_2^{\prime\prime 2}+B_{33}^{0\prime\prime}x_3^{\prime\prime 2}+2B_{23}^{0\prime\prime}x_2^{\prime\prime}x_3^{\prime\prime}=1 , \quad (48)$$

where

$$B_{11}^{0\prime\prime}=B_{11}^{0} , \quad (49a)$$

$$B_{22}^{0\prime\prime}=B_{33}^{0\prime\prime}=\tfrac{1}{2}(B_{33}^{0}+B_{22}^{0}) , \quad (49b)$$

and

$$B_{23}^{0\prime\prime}=\tfrac{1}{2}(B_{33}^{0}-B_{22}^{0}) . \quad (49c)$$

The equation of the intersection ellipse is obtained by letting $x_2^{\prime\prime}=0$ in (48):

$$B_{11}^{0\prime\prime}x_1^{\prime\prime 2}+B_{33}^{0\prime\prime}x_3^{\prime\prime 2}=1 . \quad (50)$$

Therefore

$$\Delta n_{bc}^{0}=\frac{1}{\sqrt{B_{11}^{0\prime\prime}}}-\frac{1}{\sqrt{B_{33}^{0\prime\prime}}}=n_1^0-\frac{\sqrt{2}\,n_2^0 n_3^0}{(n_2^{02}+n_3^{02})^{1/2}} . \quad (51)$$

In LTP, by substituting (47) into (4)

$$B''_{11}x''^2_1+B''_{22}x''^2_2+B''_{33}x''^2_3+2B''_{23}x''_2x''_3=1\ , \tag{52}$$

where

$$B''_{11}=B_{11}\ , \tag{53a}$$

$$B''_{22}=\tfrac{1}{2}(B_{22}+B_{33}+2B_{23})\ , \tag{53b}$$

$$B''_{33}=\tfrac{1}{2}(B_{22}+B_{33}-2B_{23})\ , \tag{53c}$$

and

$$B''_{23}=\tfrac{1}{2}(B_{33}-B_{22})\ . \tag{53d}$$

The equation of the intersection ellipse is given by letting $x''_2=0$:

$$B''_{11}x''^2_1+B''_{33}x''^2_3=1\ . \tag{54}$$

Therefore

$$\begin{aligned}\Delta n_{bc}&=\frac{1}{\sqrt{B''_{11}}}-\frac{1}{\sqrt{B''_{33}}}\\&\simeq n^0_1-\frac{\sqrt{2}\,n^0_2n^0_3}{(n^{02}_2+n^{02}_3)^{1/2}}-\frac{\sqrt{2}\,n^{02}_2n^{03}_3B_{23}}{(n^{02}_2+n^{02}_3)^{3/2}}\\&\quad+\frac{1}{2}\left\{\frac{\sqrt{2}\,n^{03}_2n^{03}_3}{(n^{02}_2+n^{02}_3)^{3/2}}(\delta B_{22}+\delta B_{33})-n^{03}_1\delta B_{11}\right\}\end{aligned} \tag{55}$$

and $\psi_{bc}=0$.

Letting $\mathbf{s}=(0,1/\sqrt{2},1/\sqrt{2})$ in both HTP and LTP

$$G_{bc}=\tfrac{1}{2}(g_{22}+g_{33})+g_{23}\ , \tag{56}$$

which becomes g_{23} in HTP.

Birefringences, gyrations and rotation angles of the indicatrix of HTP and LTP are summarized in Table I for the six different cases, where the formulas of birefringences are omitted but represented instead by the equation number for the sake of simplicity.

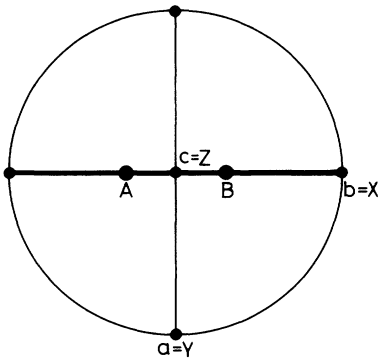

FIG. 2. Optical orientation of $BaMnF_4$ in orthorhombic system. Bold line represents an optic plane. A and B denote optic axes. Optical plane is parallel to (100) plane.

III. HAUP EXPERIMENT

Prior to the HAUP measurements, microscopic examinations of the optical nature of $BaMnF_4$ were made by using a quartz wedge. As the result, the sequence of the magnitude of the refractive indices along the crystallographic (principal) axes could be determined. Figure 2 shows the stereographic representation of the optical orientation of $BaMnF_4$ in HTP, which confirmed the validity of results of Eibschütz and Guggenheim.[1]

HAUP experiments for the above-mentioned six cases were performed by using He-Ne laser light of the wavelength of 6328 Å. The temperature range of the measurements was between 150 and 440 K in each case, the temperature stability being maintained within the accuracy of ±0.02 K. In each case, $B(0)$, retardation Δ and characteristic angle θ_0 were measured at various temperatures. These quantities are expressed as[16]

$$\Delta=\frac{2\pi d}{\lambda}[\Delta n^2+(G/\bar{n})^2]^{1/2}\ , \tag{57a}$$

$$B(0)=(\gamma-2k)\sin\Delta+2\delta\Upsilon\cos^2(\Delta/2)\ , \tag{57b}$$

TABLE I. Birefringences, gyrations, and rotation angles of indicatrix for six cases.

Case	Birefringence		Gyration		Rotation angle of indicatrix	
	HTP	LTP	HTP	LTP	HTP	LTP
1	(3)	(9)	0	g_{11}	0	$\frac{n^{02}_2n^{02}_3B_{23}}{n^{02}_2-n^{02}_3}$
2	(13)	(14)	0	g_{22}	0	0
3	(17)	(18)	0	g_{33}	0	0
4	(24)	(31)	0	$\frac{1}{2}(g_{11}+g_{22})+g_{12}$	0	$\frac{\sqrt{2}(n^0_1n^0_2n^0_3)^2B_{23}}{2n^{02}_1n^{02}_2-(n^{02}_2n^{02}_3+n^{02}_1n^{02}_3)}$
5	(38)	(44)	0	$\frac{1}{2}(g_{11}+g_{33})+g_{13}$	0	$\frac{\sqrt{2}(n^0_1n^0_2n^0_3)^2B_{23}}{n^{02}_2n^{02}_3+n^{02}_1n^{02}_2-2n^{02}_1n^{02}_3}$
6	(51)	(55)	g_{23}	$\frac{1}{2}(g_{22}+g_{33})+g_{23}$	0	0

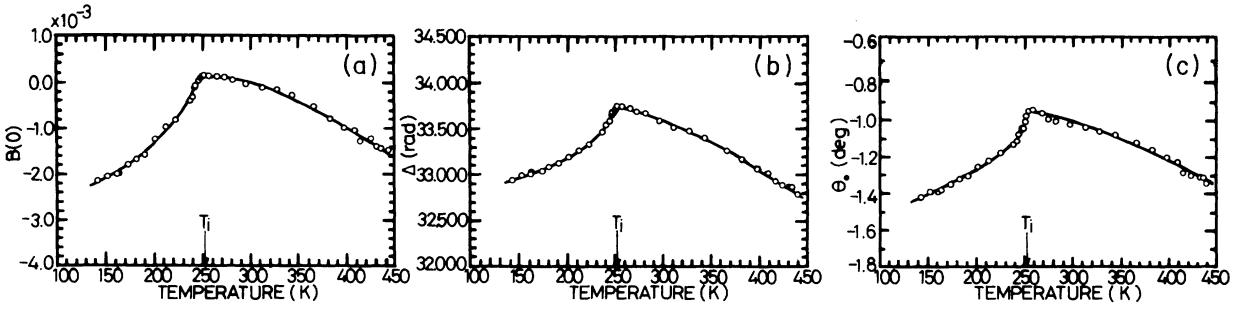

FIG. 3. Temperature dependences of (a) $B(0)$, (b) Δ, and (c) θ_0 for Case-1 of $BaMnF_4$.

and

$$\theta_0 = -\tfrac{1}{2}(p+q)\cot(\Delta/2) - \tfrac{1}{2}\delta\Upsilon + \psi \ . \tag{57c}$$

Here d designates thickness of the specimen, k ellipticity of the elliptically polarized wave traveling in the specimen, ψ rotation angle of the indicatrix, and $\bar{n}$ mean refractive index. $\gamma = p - q$ and $\delta\Upsilon$ are the major systematic errors; where p and q represent the parasitic ellipticities of the polarizer and analyzer, respectively, and $\delta\Upsilon$ the deflection angle from the true crossed Nicols condition. Equation (57b) becomes

$$B(0)/\sin\Delta = \gamma + \delta\Upsilon\cot(\Delta/2) \ , \tag{57d}$$

when $k = 0$. That is to say, $B(0)/\sin\Delta$ changes linearly with respect to $\cot(\Delta/2)$ when the crystal is optically inactive. The similar relation is held for θ_0 when $\psi = 0$. Making use of these two relations the systematic errors p, q, and $\delta\Upsilon$ can be properly evaluated as described in details in Ref. 16.

A. Case-1

A specimen with flat (100) planes of the area of 1.20×1.65 mm^2 and thickness of 0.107 mm was prepared. The specimen was firstly investigated at a diagonal position of the microscope. When the X' axis of the quartz wedge was parallel to the x_2 axis of the specimen, the retardation of both crystals was found to be added, while parallel to the x_3 axis the retardation subtracted. Thus it was confirmed that the x_2 and x_3 axes correspond to X' and Z' axes, respectively. Furthermore, the temperature change of $\Delta n_a = n_3 - n_2$ was measured by using the quartz wedge. The result was satisfactorily agreed with that derived by HAUP method which is to be described below.

The temperature dependences of $B(0)$, Δ, and θ_0 are shown in Figs. 3(a)–3(c), $B(0)/\sin\Delta$ and θ_0 in HTP clearly change linearly with respect to $\cot(\Delta/2)$, as depicted in Figs. 4(a) and 4(b). From these relations the systematic errors were determined; $p = 9.14 \times 10^{-3}$, $q = 7.98 \times 10^{-3}$, and $\delta\Upsilon = -2.40 \times 10^{-3}$. By using these values, k was derived as a function of T as shown in Fig. 5. Then the temperature changes of G_a and Δn_a were derived as represented in Figs. 6 and 7. As can be seen from Fig. 6, G_a is zero in HTP, but appears in LTP. It was found that Δn_a in HTP increased with decreasing temperatures, contrary to the previous reports.[13,14] By combining temperature dependences of Δ and θ_0 which are represented in Figs. 3(b) and 3(c), temperature dependence of ψ_a was deduced as shown in Fig. 8. It was clearly seen that the indicatrix rotates in LTP depending strongly on T.

B. Case-2

A specimen with (010) planes of the area of 1.90×2.80 mm^2 and thickness of 0.168 mm was prepared. By the same microscopic examination as in Case-1, the x_1 and x_3 axes were confirmed to be X' and Z' axes, respective-

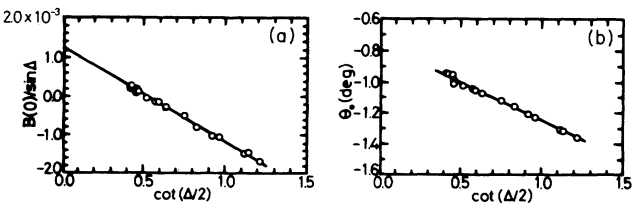

FIG. 4. Relations of (a) $B(0)/\sin\Delta$ and (b) θ_0 with respect to $\cot(\Delta/2)$, for Case-1 of the high temperature phase of $BaMnF_4$.

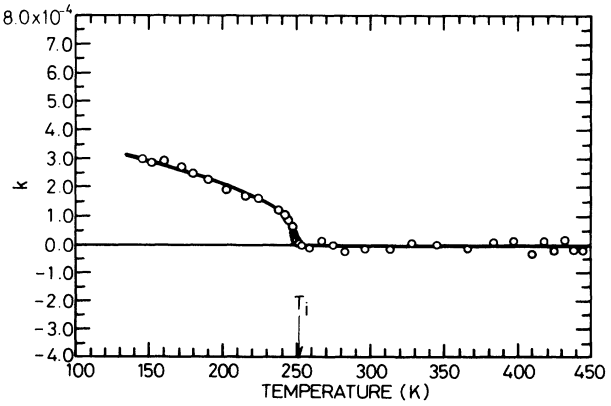

FIG. 5. Temperature dependence of ellipticity k for Case-1 of $BaMnF_4$.

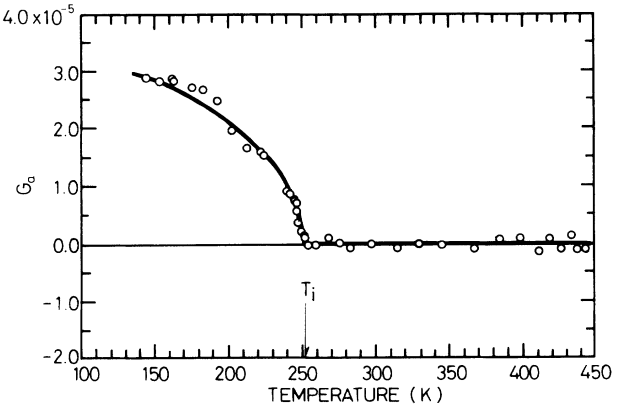

FIG. 6. Temperature dependence of gyration G_a of $BaMnF_4$.

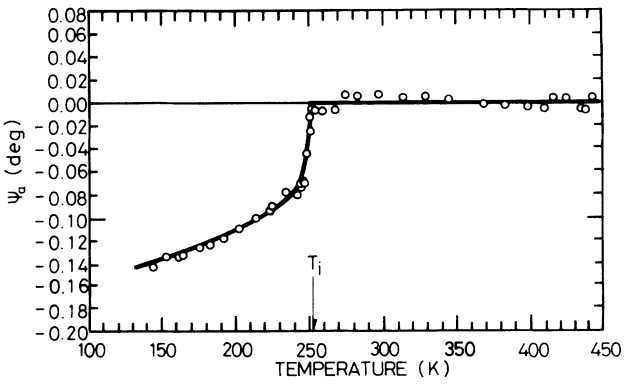

FIG. 8. Temperature dependence of rotation angle of indicatrix, ψ_a, of $BaMnF_4$.

ly. The preliminary birefringence measurement by using the quartz wedge also provided nearly the same temperature dependence as that measured by HAUP.

In Figs. 9(a)–9(c), temperature dependences of $B(0)$, Δ, and θ_0 are shown. From the linear relations of $B(0)/\sin\Delta$ and θ_0 of HTP with respect to $\cot(\Delta/2)$, the systematic errors were evaluated; $p=-1.13\times10^{-3}$, $q=-2.10\times10^{-3}$, and $\delta\Upsilon=-3.4\times10^{-4}$. After determining the temperature dependence of k, as shown in Fig. 9(d), G_b and Δn_b were acquired as a function of T, as depicted in Figs. 10 and 11.

By using the systematic errors and temperature dependences of Δ and θ_0, the temperature dependence of ψ_b was deduced as shown in Fig. 12.

C. Case-3

A specimen with flat (001) planes of the area of 1.82×2.50 mm^2 and thickness of 0.489 mm was prepared. The temperature dependences of $B(0)$, Δ, and θ_0 are shown in Figs. 13(a)–13(c), respectively. The systematic errors were determined as $p=-2\times10^{-5}$, $q=-5.7\times10^{-4}$, and $\delta\Upsilon=4.9\times10^{-4}$. With these values, the temperature dependence of k was determined as shown in Fig. 13(d). Then the temperature dependences of G_c, Δn_c, and ψ_c were acquired as depicted in Figs. 14, 15, and 16.

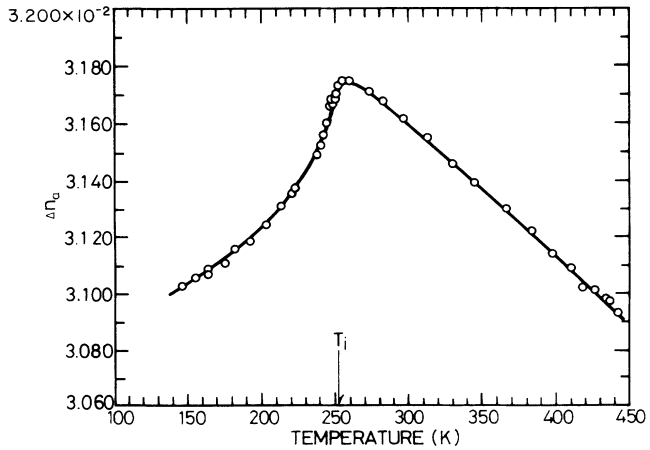

FIG. 7. Temperature dependence of birefringence Δn_a of $BaMnF_4$.

D. Case-4

A specimen with the flat planes which were parallel to the x_3 axis and perpendicular to s of Case-4 was prepared, the area being 2.13×1.54 mm^2 and thickness 0.199 mm, respectively.

Temperature dependences of $B(0)$, Δ, θ_0, and k are depicted in Figs. 17(a)–17(d), respectively. The systematic errors were determined as $p=4.5\times10^{-4}$, $q=1.9\times10^{-4}$, and $\delta\Upsilon=-2.9\times10^{-4}$. The temperature dependences of G_{ab}, Δn_{ab}, and ψ_{ab} are shown in Figs. 18, 19, and 20.

E. Case-5

A specimen with the flat planes which were parallel to the x_2 axis and perpendicular to s of Case-5 was prepared; the area and thickness being 1.52×1.76 mm^2 and 0.345 mm, respectively. The temperature dependences of $B(0)$, Δ, θ_0, and k are depicted in Figs. 21(a)–21(d), respectively. The systematic errors were $p=-1.79\times10^{-3}$, $q=-1.91\times10^{-3}$, and $\delta\Upsilon=1.90\times10^{-4}$. Temperature dependences of G_{ca}, Δn_{ca}, and ψ_{ca} are shown in Figs. 22, 23, and 24.

F. Case-6

A specimen with the flat planes which were parallel to the x_1 axis and perpendicular to s of Case-6 was prepared; the area and thickness being 1.99×1.62 mm^2 and 0.169 mm, respectively. Temperature dependences of $B(0)$, Δ, θ_0, and k are depicted in Figs. 25(a)–25(d), respectively. From the symmetry it was expected that G_{bc} was nonzero in both phases. In that case, the linear relation of $B(0)/\sin\Delta$ versus $\cot(\Delta/2)$ cannot hold, and ac-

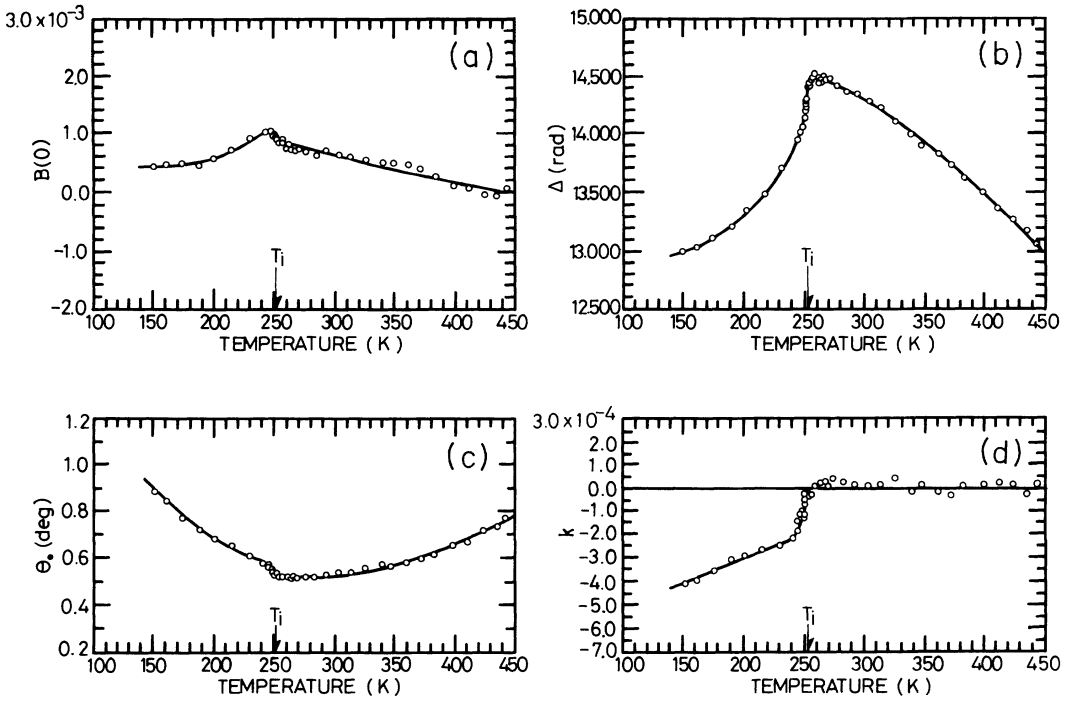

FIG. 9. Temperature dependences of (a) $B(0)$, (b) Δ, (c) θ_0, and (d) k for Case-2 of $BaMnF_4$.

cordingly the systematic errors cannot be obtained straightforwardly unlike the previous five cases. Although this had been the most difficult problem in the HAUP method, we have already solved it successfully.[21] In the present case, $LiNbO_3$ was taken as the standard specimen. The linear relations of $B(0)/\sin\Delta$ and θ_0 with respect to $\cot(\Delta/2)$ were definitely held in this crystal as indicated in Figs. 26(a) and 26(b). From the intercept of the figure (a) and the derivative of the figure (b), $\hat{p}-q'$ and $\hat{p}+q'$ were derived, respectively, where $\hat{p}$ designates the common ellipticity of the polarizer of $LiNbO_3$ and $BaMnF_4$ systems and q' the ellipticity of the analyzer of

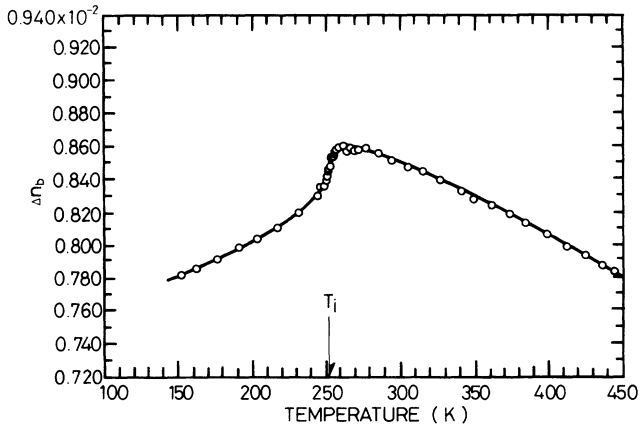

FIG. 11. Temperature dependence of birefringence Δn_b of $BaMnF_4$.

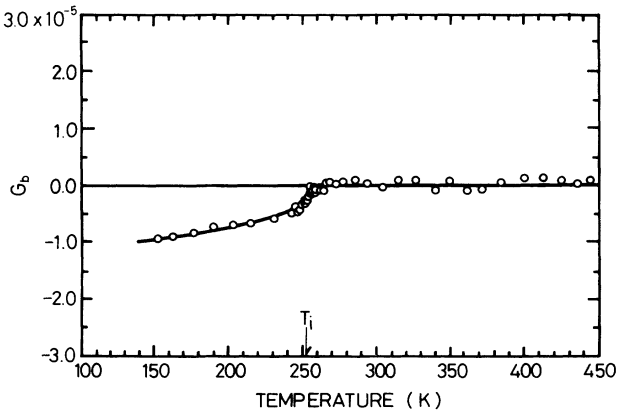

FIG. 10. Temperature dependence of gyration G_b of $BaMnF_4$.

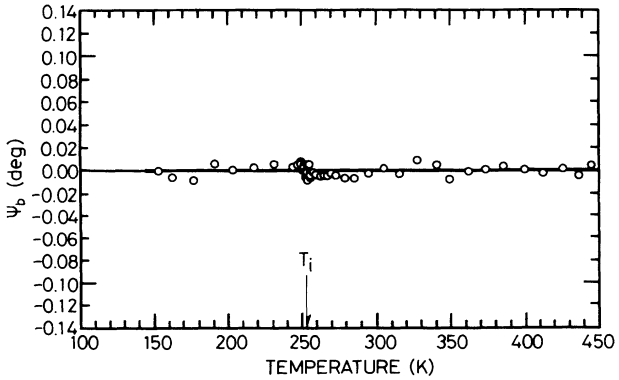

FIG. 12. Temperature dependence of rotation angle of indicatrix, ψ_b, of $BaMnF_4$.

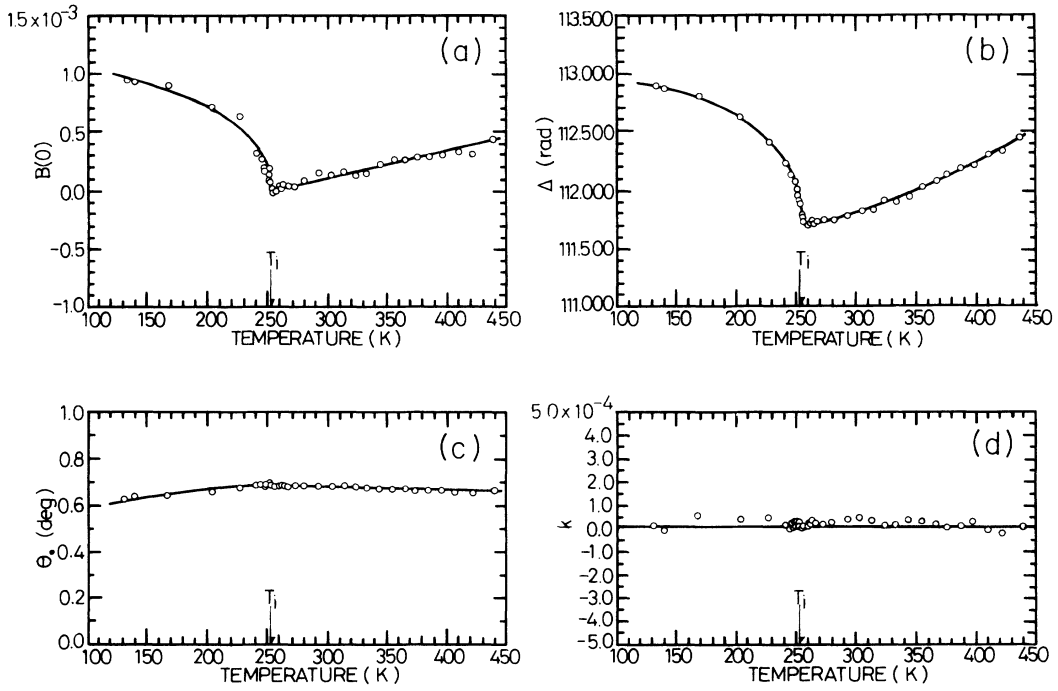

FIG. 13. Temperature dependences of (a) $B(0)$, (b) Δ, (c) θ_0, and (d) k for Case-3 of $BaMnF_4$.

$LiNbO_3$ system. Thus $\hat{p}$ was obtained separately as -8×10^{-5}. From the derivative of the linear relationship between θ_0 and $\cot(\Delta/2)$ of $BaMnF_4$, $\hat{p}+q$ of this optical system was determined as 2.44×10^{-3}. Thus $\gamma=\hat{p}-q$ of this system was determined as -2.60×10^{-3}. $\delta\Upsilon$ can be obtained from the value of $B(0)$ for the case of $\Delta=2n\pi$, where n represents an integer. The relation between $B(0)$ and Δ is indicated in Fig. 27, where $\delta\Upsilon$ was evaluated as 2.5×10^{-4}.

After determining k by these systematic errors, temperature dependences of G_{bc}, Δn_{bc}, and ψ_{bc} were derived and shown in Figs. 28, 29, and 30.

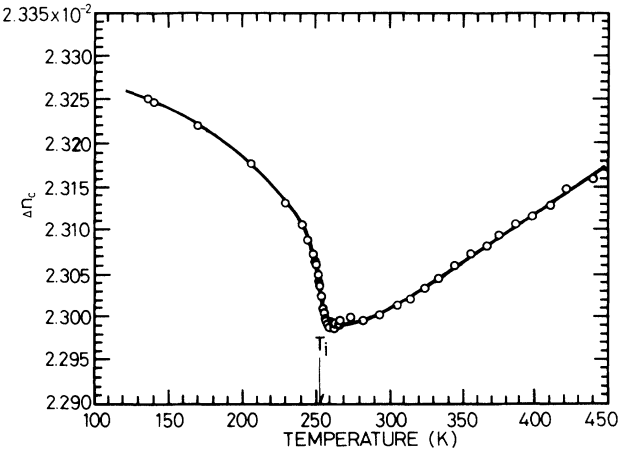

FIG. 15. Temperature dependence of birefringence Δn_c of $BaMnF_4$.

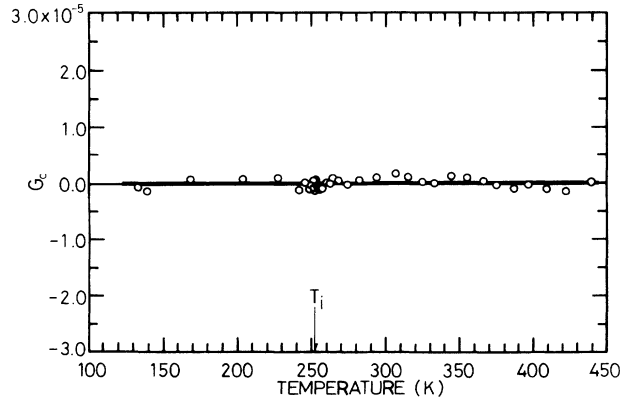

FIG. 14. Temperature dependence of gyration G_c of $BaMnF_4$.

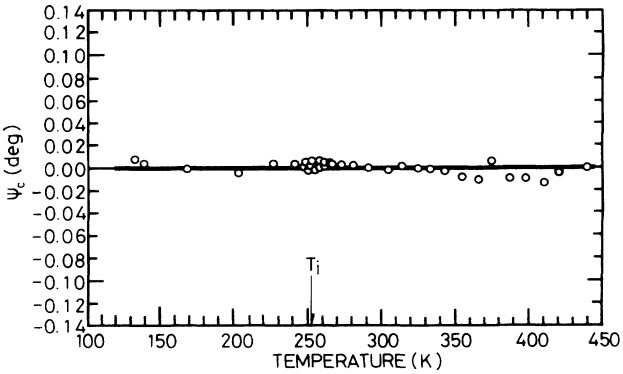

FIG. 16. Temperature dependence of rotation angle of indicatrix, ψ_c, of $BaMnF_4$.

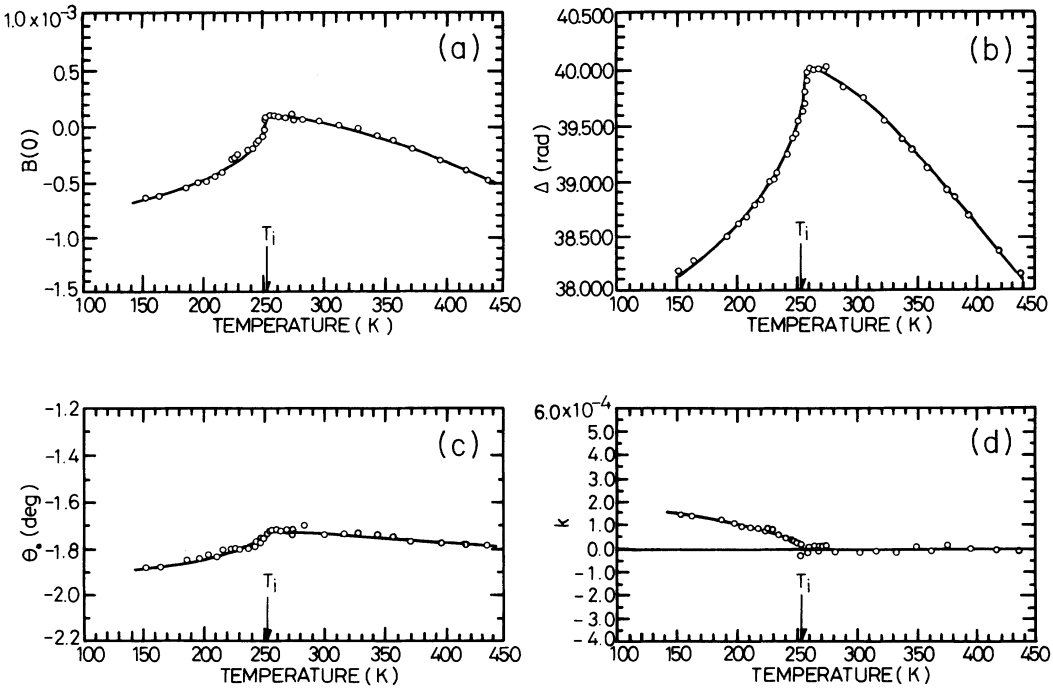

FIG. 17. Temperature dependences of (a) $B(0)$, (b) Δ, (c) θ_0, and (d) k for Case-4 of $BaMnF_4$.

IV. EXPERIMENTAL RESULTS

Here we will summarize our experimental results.

From Figs. 6, 10, and 14, it is seen that $g_{11}=g_{22}=g_{33}=0$ in HTP. Accordingly from Figs. 18 and 22, $g_{12}=g_{13}=0$ in the same phase. Figure 28 indicates that only g_{23} remains nonzero in HTP. These facts confirm the validity of the representation of the gyration tensor of HTP shown in Fig. 1.

Temperature dependences of g_{11} and g_{22} in LTP are shown in Figs. 6 and Fig. 10. g_{33} is always zero as shown in Fig. 14. g_{12} can be estimated by subtracting $\frac{1}{2}(g_{11}+g_{22})$ from G_{ab} shown in Fig. 18. Also g_{13} can be evaluated by subtracting $\frac{1}{2}g_{11}$ from G_{ca} of Fig. 22. Both

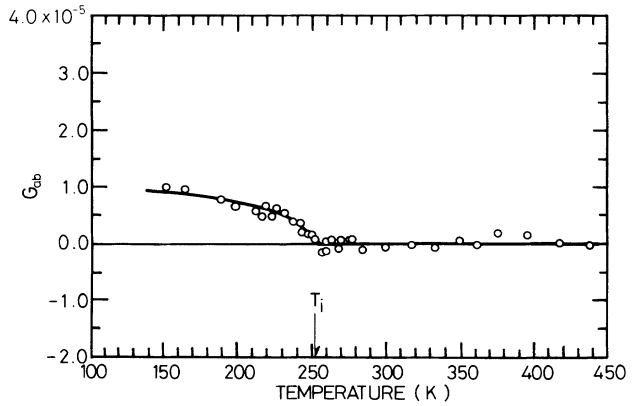

FIG. 18. Temperature dependence of gyration G_{ab} of $BaMnF_4$.

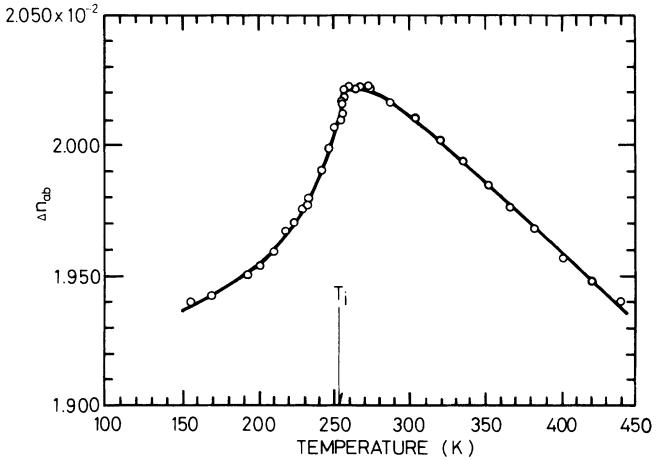

FIG. 19. Temperature dependence of birefringence Δn_{ab} of $BaMnF_4$.

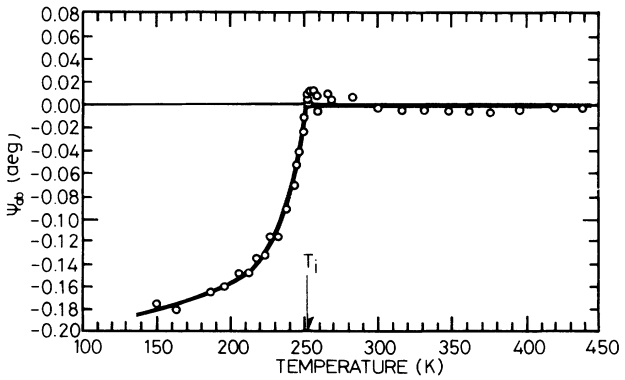

FIG. 20. Temperature dependence of rotation angle of indicatrix, ψ_{ab}, of $BaMnF_4$.

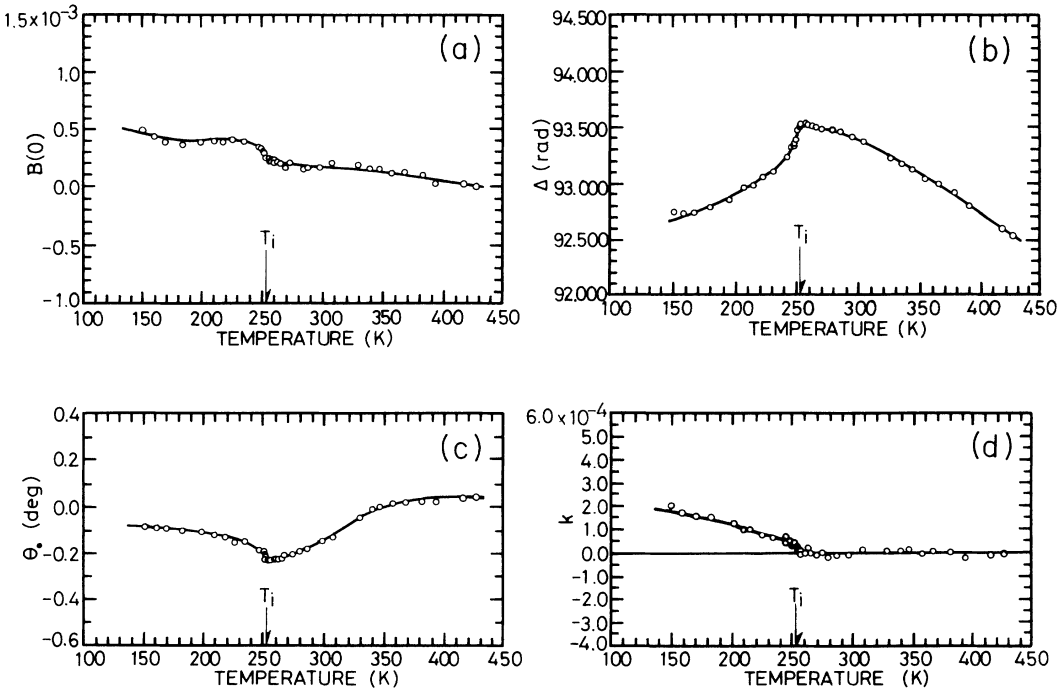

FIG. 21. Temperature dependences of (a) $B(0)$, (b) Δ, (c) θ_0, and (d) k for Case-5 of $BaMnF_4$.

results are indicated in Fig. 31, i.e., $g_{12}=g_{13}=0$ in LTP. The temperature dependence of g_{23} in LTP was obtained by subtracting $\frac{1}{2}g_{22}$ of Fig. 10 from G_{bc} of Fig. 28 and indicated in Fig. 32. Summarizing the above results, temperature changes of the gyration tensor components of $BaMnF_4$ are represented in Fig. 33.

The rotations of the indicatrix were detected to occur in ψ_a (Fig. 8), ψ_{ab} (Fig. 20), and ψ_{ca} (Fig. 24), but not in ψ_b (Fig. 12), ψ_c (Fig. 16), and ψ_{bc} (Fig. 30) at all. These facts unequivocally indicate that the indicatrix rotates only around the a axis by the presence of B_{23} component. The temperature dependence of B_{23} was obtained from the values of ψ_a, ψ_{ab}, and ψ_{ca} at the measured tempera-

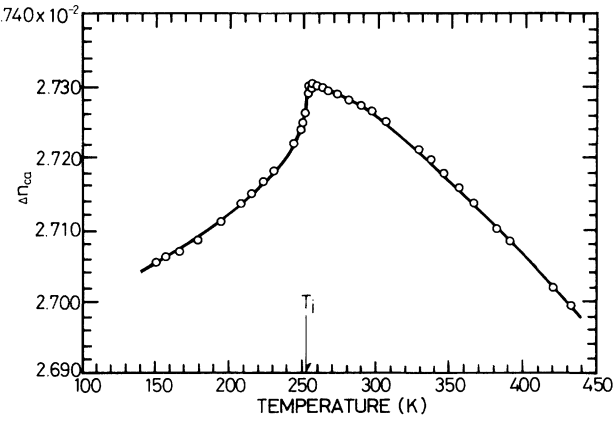

FIG. 23. Temperature dependence of birefringence Δn_{ca} of $BaMnF_4$.

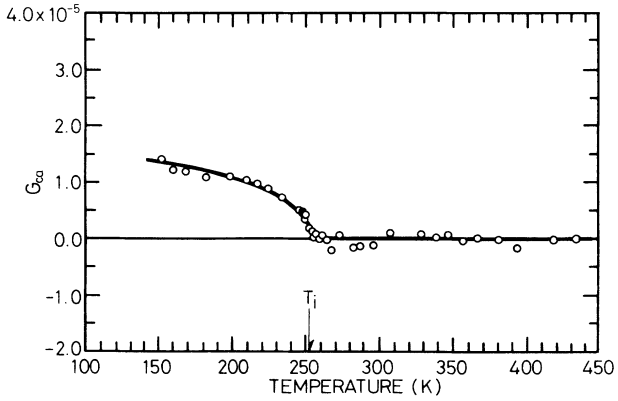

FIG. 22. Temperature dependence of gyration G_{ca} of $BaMnF_4$.

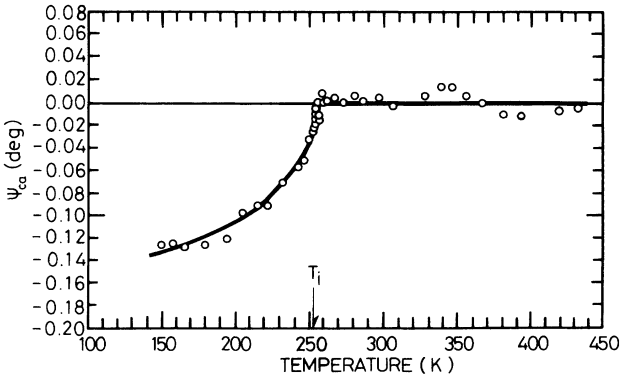

FIG. 24. Temperature dependence of rotation angle of indicatrix, ψ_{ca}, of $BaMnF_4$.

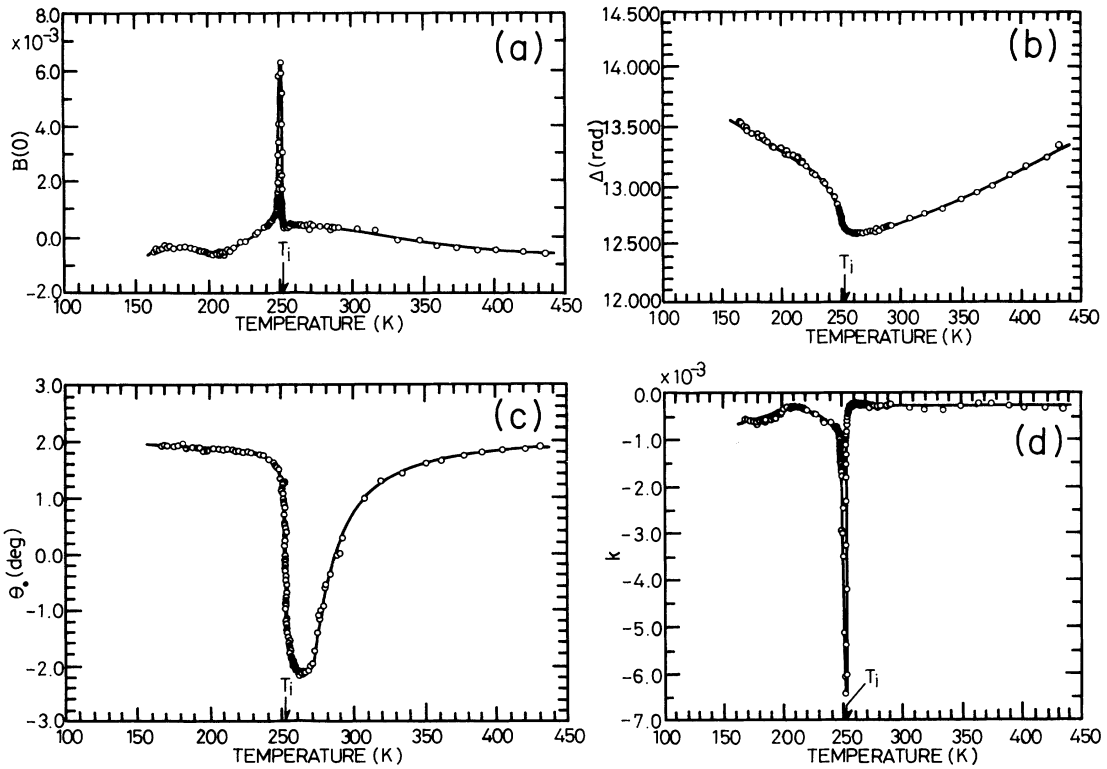

FIG. 25. Temperature dependences of (a) $B(0)$, (b) Δ, (c) θ_0, and (d) k for Case-6 of $BaMnF_4$.

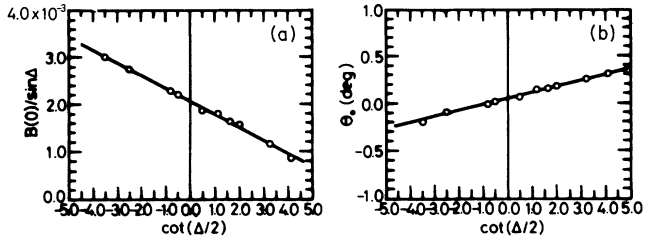

FIG. 26. Relations of (a) $B(0)/\sin\Delta$ and (b) θ_0 with respect to $\cot(\Delta/2)$ of $LiNbO_3$ used as the standard specimen.

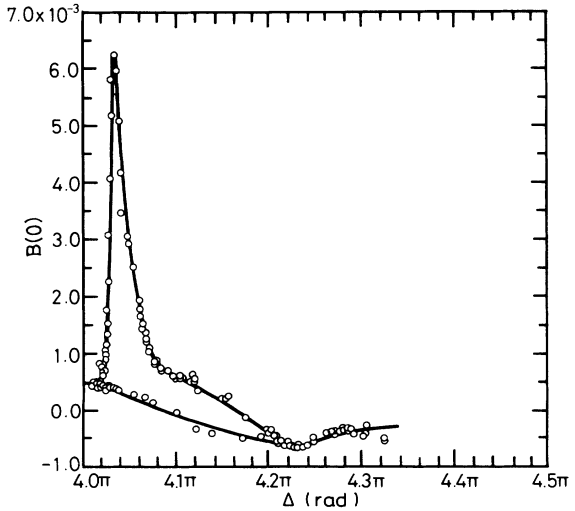

FIG. 27. Relationship between $B(0)$ and Δ for Case-6 of $BaMnF_4$. Extrapolated value of $B(0)$ is evaluated as 5.0×10^{-4} for the case of $\Delta=4.0\pi$.

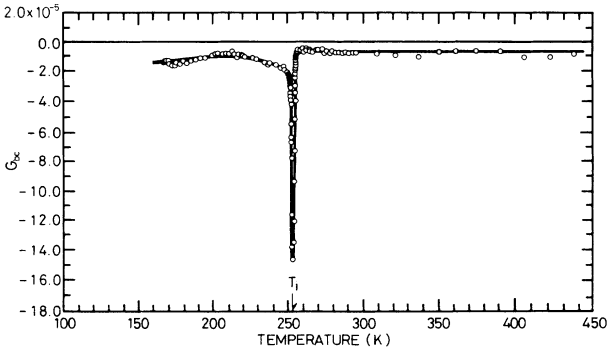

FIG. 28. Temperature dependence of gyration G_{bc} of $BaMnF_4$.

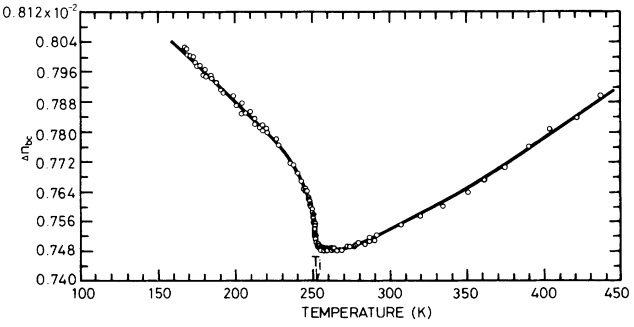

FIG. 29. Temperature dependence of birefringence Δn_{bc} of $BaMnF_4$.

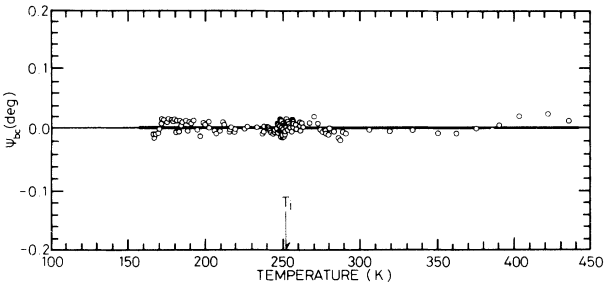

FIG. 30. Temperature dependence of rotation angle of indicatrix, ψ_{bc}, of $BaMnF_4$.

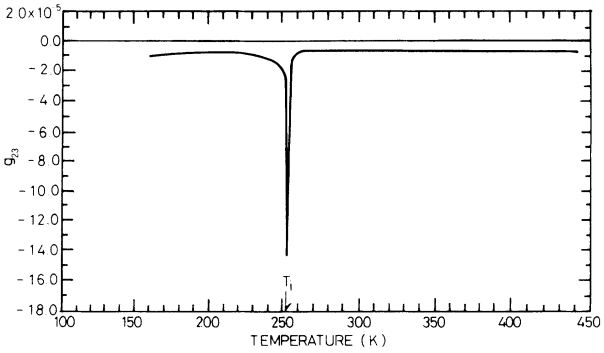

FIG. 32. Temperature dependence of gyration tensor component g_{23} of $BaMnF_4$.

tures. They are shown in Fig. 34, where the superscripts designate the relevant rotation angles and $\overline{B_{23}}$ the mean value. It is seen in the figure that the coincidence of each branch is satisfactory.

Finally the temperature dependences of Δn are summarized in Fig. 35.

V. DISCUSSIONS

We successfully measured the gyration tensor components of $BaMnF_4$ in the temperature range containing IC phase transition. So it will be of interest to look at the relationship between the change of the optical activity and the IC phase transition.

As only g_{23} exists commonly in both phases, we will investigate the change of the gyration in the (100) plane. In HTP, the gyration G is expressed as follows, when the light beam with the wave vector $\mathbf{s}=(0,l_2,l_3)$ is incident on the crystal:

$$G=2g_{23}l_2l_3=g_{23}\sin(2\theta_2)\ , \tag{58}$$

where θ_2 is the angle which makes with the x_2 axis, and $g_{23}<0$. Therefore the negatively maximum value of G will be observed at $\theta_2=\pi/4$, and the positively maximum

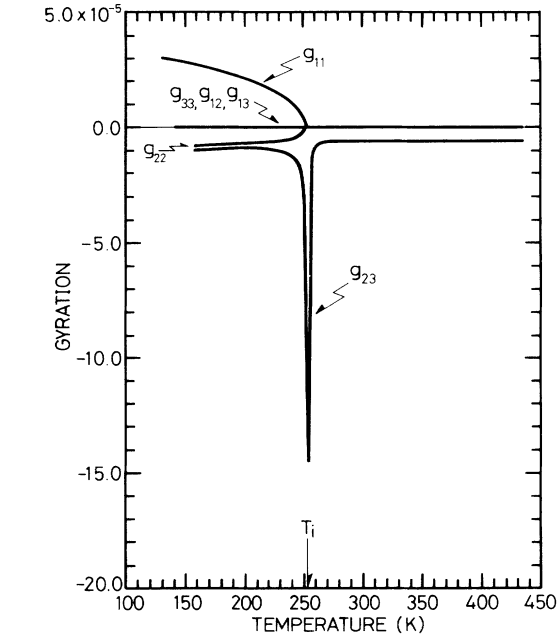

FIG. 33. Temperature variations of all the gyration tensor components of $BaMnF_4$.

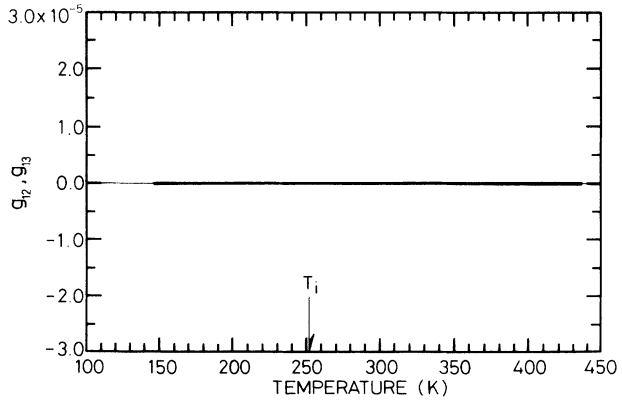

FIG. 31. Temperature dependences of gyration tensor components g_{12} and g_{13} of $BaMnF_4$.

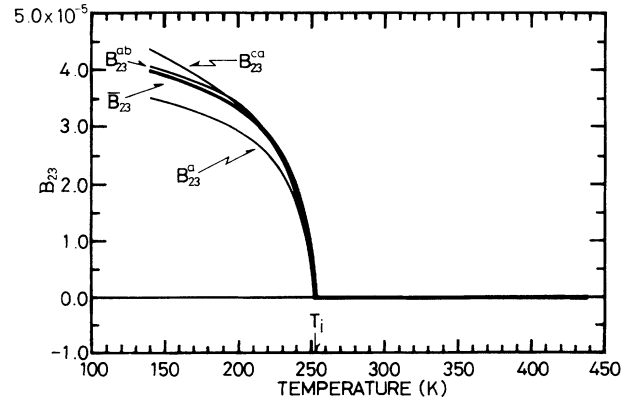

FIG. 34. Temperature variations of a dielectric impermeability tensor component B_{23}, where superscripts, *a*, *ab*, and *ca* express the relevant rotations for Case-1, Case-4, and Case-5, respectively, and $\overline{B_{23}}$ the mean value.

value at $\frac{3}{4}\pi$. The section of the gyration surface[27] of HTP with the (x_2,x_3) plane is depicted in Fig. 36(a), where the negative radius vectors are drawn black and the positive radius vectors white. It must be noticed in the figure that the two white and two black ovoid sections are interrelated by the mutually crossed mirror planes and a diad axis which are commonly parallel to the x_1 axis. In this case, g_{11} is forbidden to occur by the symmetry. Our experiment clarified that the shape and orientation of the ovoid sections did not change until the temperature approached very closely T_i. However, the shape of the ovoid sections suddenly expand near T_i as depicted in Fig. 36(b), because g_{23} manifests a sharp peak at T_i. It is reasonable to consider that g_{23} becomes infinite in essence at T_i but, in reality, was measured as a definite value under the effect of the higher order terms. As the expansion of the ovoid sections becomes infinite at T_i, effect of the mirror planes collapses. Thus it is very interesting to interpret that the divergence of g_{23} plays a role of making continuous.

In LTP, the mirror planes disappear, and only a diad axis remains to exist. Then g_{11} can be generated and the gyration surface can be rotated in this reduced symmetry. We really observed $g_{11}(>0)$ and $g_{22}(<0)$ below T_i. G in the (100) plane can be expressed as

$$\begin{aligned} G &= g_{22}l_2^2 + 2g_{23}l_2l_3 \\ &= \tfrac{1}{2}g_{22}[1+\cos(2\theta_2)] + g_{23}\sin(2\theta_2) \\ &= \sqrt{(1/4)g_{22}^2 + g_{23}^2}\cos(2\theta_2+\varphi) + \tfrac{1}{2}g_{22} , \end{aligned} \tag{59}$$

where

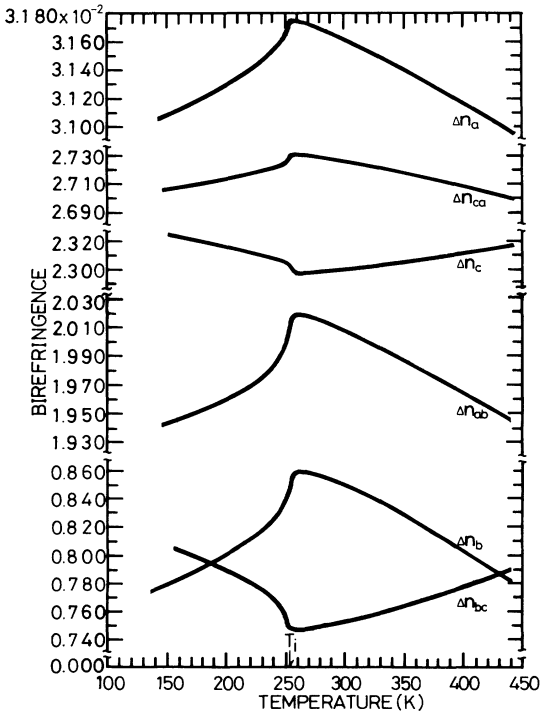

FIG. 35. Temperature variations of the birefringences for six cases, where subscripts of Δn correspond to the relevant cases.

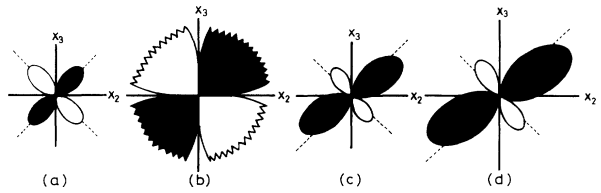

FIG. 36. Sections of the gyration surface of $BaMnF_4$ with (100) plane. (a) 260 K, (b) 253 K($\simeq T_i$), (c) 230 K, and (d) 160 K.

$$\cos\varphi = \frac{g_{22}}{\sqrt{g_{22}^2+4g_{23}^2}} , \tag{60a}$$

$$\sin\varphi = -\frac{2g_{23}}{\sqrt{g_{22}^2+4g_{23}^2}} , \tag{60b}$$

and

$$\tan\varphi = -\frac{2g_{23}}{g_{22}} . \tag{60c}$$

The negatively maximum value of G will appear at θ_2, which satisfies the condition of $\cos(2\theta_2+\varphi)=-1$, i.e., $\theta_2=\pi/2-\varphi/2$. On the other hand, the positively maximum value of G occurs at $\theta_2'=\pi-\varphi/2$. As $\tan\varphi$ is negative, φ can be expressed as

$$\varphi = \frac{\pi}{2}+\beta . \tag{61}$$

Then

$$\theta_2 = \frac{\pi}{4}-\frac{\beta}{2} \tag{62a}$$

and

$$\theta_2' = \frac{3}{4}\pi-\frac{\beta}{2} . \tag{62b}$$

In HTP, θ_2 and θ_2' are always $\pi/4$ and $3/4\pi$. In LTP, with the increase of the magnitude of g_{22}, θ_2, and θ_2' decrease and the two kinds of ovoid sections rotate clockwise simultaneously. Using Fig. 33 change of θ_2 could be

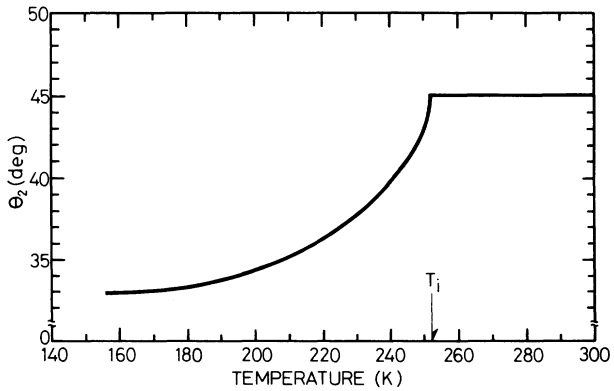

FIG. 37. Temperature dependence of θ_2.

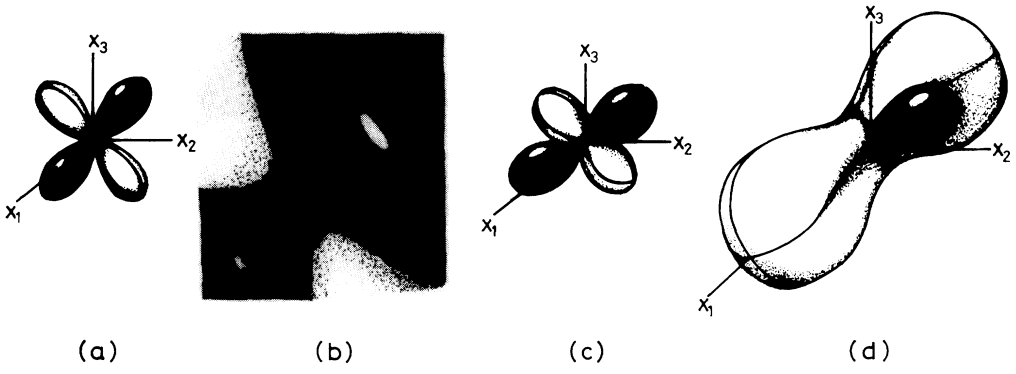

FIG. 38. Schematical representation of the change of the gyration surface of $BaMnF_4$ at various temperatures. (a) 260 K, (b) 253 K($\simeq T_i$), (c) 230 K, and (d) 160 K.

deduced as depicted in Fig. 37. The sections of the gyration surface at 230 and 160 K are drawn in Figs. 36(c) and 36(d).

Below T_i, g_{11} appears and increases with decreasing temperatures as shown in Fig. 33. Total changes of the gyration surface with decreasing temperature are schematically depicted in Fig. 38; (a) at 260 K ($\mathbf{C}_{2v}$), (b) 253 K ($\simeq T_i$), (c) 230 K ($\mathbf{C}_2$), and (d) 160 K ($\mathbf{C}_2$).

As has already been mentioned, the sharp peak of g_{23} makes the transition of $BaMnF_4$ perfectly second order. It is an interesting problem to investigate whether the gyration always manifests such a phenomenon when the transition between two optically active phases is of second order. However, we must wait for the accumulation of much more experimental data for getting the conclusion.

At last, we revealed the temperature changes of the rotation angle ψ_a of the indicatrix and the rotation angle $\beta/2$ of the gyration surface, in addition to the lattice parameter α angle.[11] It is remarkable that $\beta/2$ is 2 orders of magnitude larger than ψ_a, which is 1 order larger than α. This fact indicates that gyrations are affected very sensitively by the change of the order parameter.

Our results on the birefringences do not agree with those of Régis *et al.*,[12] Pisarev *et al.*,[13] and Schäfer *et al.*[14] except Δn_c. Comparisons are made in Fig. 39 between the results of Schäfer *et al.* and of ours, where the appropriate values are put to the three birefringences of Schäfer *et al.* since the absolute values were not shown in their report. Although both reports agree in Δn_c, temperature dependences of Δn_a and Δn_b are wholly opposite.

Deflections of the three major birefringences, $\delta(\Delta n_a)$, $\delta(\Delta n_b)$, and $\delta(\Delta n_c)$, in LTP from those in HTP are shown in Fig. 40. Remarkable fluctuations of the refractive indices are observed above T_i, as were already mentioned in previous reports.[13,14] From the figure, $\delta(\Delta n_a)=\delta n_3-\delta n_2<0$, $\delta(\Delta n_b)=\delta n_3-\delta n_1<0$, and $\delta(\Delta n_c)=\delta n_1-\delta n_2>0$. Then it can be concluded that $\delta n_1>\delta n_2>\delta n_3$. In other words, the change of birefringence is maximum along the IC axis when the order parameter appears. It is necessary to add that the gyration component takes place along this axis below T_i and develops conspicuously.

In summing up the present work, we find the various peculiar properties manifested by $BaMnF_4$ fascinating and intriguing. Among these properties, the sharp peak

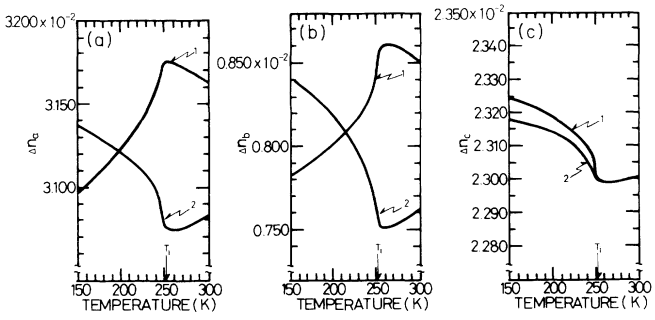

FIG. 39. Comparisons of temperature dependences of birefringences for (a) Δn_a, (b) Δn_b, and (c) Δn_c. Present results are designated by 1 and Schäfer *et al.*'s by 2.

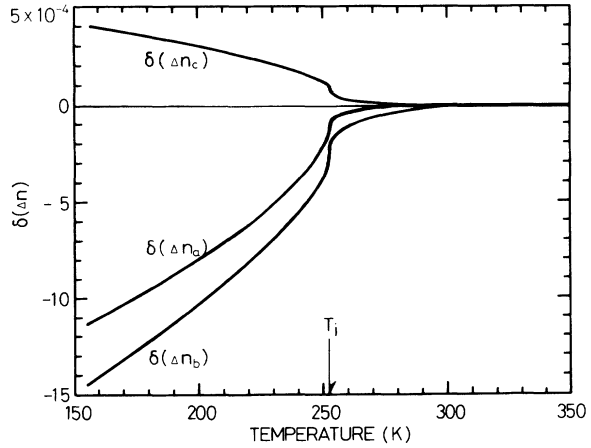

FIG. 40. Temperature dependences of the deflections of birefringences $\delta(\Delta n)$ of the low temperature phase from those of the high temperature phase.

of a gyration tensor component at the transition, and the large rotation of gyration surface in the IC phase, will be useful for understanding the IC phase transition of $BaMnF_4$ from a different viewpoint.

ACKNOWLEDGMENT

The authors thank Miss M. Higano and Miss N. Takahashi for their contributions to the present experiments.

[1]M. Eibschütz and H. J. Guggenheim, Solid State Commun. **6**, 737 (1968).

[2]J. F. Scott, Rep. Prog. Phys. **12**, 1055 (1979).

[3]D. E. Cox, S. M. Shapiro, R. A. Cowley, M. Eibschütz, and H. J. Guggenheim, Phys. Rev. B **19**, 5754 (1979).

[4]E. T. Keve, S. C. Abrahams, and J. L. Bernstein, J. Chem. Phys. **51**, 4928 (1969).

[5]For instance, Y. Ishibashi, in *Incommensurate Phases in Dielectrics,* edited by R. Blinc and A. P. Levanyuk (North-Holland, Amsterdam, 1986), Vol. 2, p. 49.

[6]D. E. Cox, S. M. Shapiro, R. J. Nelmes, T. W. Ryan, H. J. Bleif, R. A. Cowley, M. Eibschütz, and H. J. Guggenheim, Phys. Rev. B **28**, 1640 (1983).

[7]M. Barthès-Régis, R. Almairac, P. St.-Grégoire, C. Filippini, U. Steigenberger, J. Nouet, and J. Y. Gesland, J. Phys. (Paris) Lett. **44**, 829 (1983).

[8]V. Dvořák and J. Fousek, Phys. Status Solidi A **61**, 99 (1980).

[9]T. W. Ryan, J. Phys. C **19**, 1097 (1986).

[10]P. St.-Grégoire, R. Almairac, A. Freund, and J. Y. Gesland, Ferroelectrics **67**, 15 (1986).

[11]T. Ogawa, T. Kameshima, S. Miura, H. Munakata, H. Takano, Y. Koyano, J. Kobayashi, and W. Kleemann, Ferroelectrics **105**, 207 (1990).

[12]M. Régis, M. Candille, and P. St.-Grégoire, in *Recent Development in Condensed Matter Physics,* edited by J. T. Devreese *et al.* (Plenum, New York, 1981), Vol. 4, p. 107.

[13]R. V. Pisarev, B. B. Krichevtzov, P. A. Markovin, O. Yu. Korshunov, and J. F. Scott, Phys. Rev. B **28**, 2677 (1983).

[14]F. J. Schäfer, W. Kleemann, and T. Tsuboi, J. Phys. C **16**, 3987 (1983).

[15]P. St.-Grégoire, W. Kleemann, F. J. Schäfer, and J. Moret, J. Phys. (Paris) **49**, 463 (1988).

[16]J. Kobayashi, H. Kumomi, and K. Saito, J. Appl. Crystallogr. **19**, 377 (1986).

[17]J. Kobayashi, K. Saito, H. Fukase, and K. Matsuda, Phase Transitions **12**, 225 (1988).

[18]K. Saito, H. Sugiya, and J. Kobayashi, J. Appl. Phys. **68**, 732 (1990).

[19]J. Kobayashi, Phys. Rev. B **42**, 8332 (1990).

[20]J. Kobayashi and Y. Uesu, J. Appl. Crystallogr. **16**, 204 (1983).

[21]J. Kobayashi, T. Asahi, S. Takahashi, and A. M. Glazer, J. Appl. Crystallogr. **21**, 479 (1988).

[22]T. Asahi, K. Uchino, J. Kobayashi and W. Kleemann, Ferroelectrics **94**, 329 (1989).

[23]T. Asahi, K. Uchino, M. Tomizawa, J. Kobayashi and W. Kleemann, Ferroelectrics **105**, 213 (1990).

[24]P. M. de Wolff, T. Janssen, and A. Janner, Acta Crystallogr. A **37**, 625 (1981).

[25]Ph. Sciau, J. Lapasset, D. Grebille, and J. F. Berar, Acta Crystallogr. B **44**, 108 (1988).

[26]J. F. Nye, *Physical Properties of Crystals* (Clarendon, Oxford, England, 1985).

[27]A. V. Shubnikov, *Principles of Optical Crystallography* (Consultant Bureau, New York, 1960).

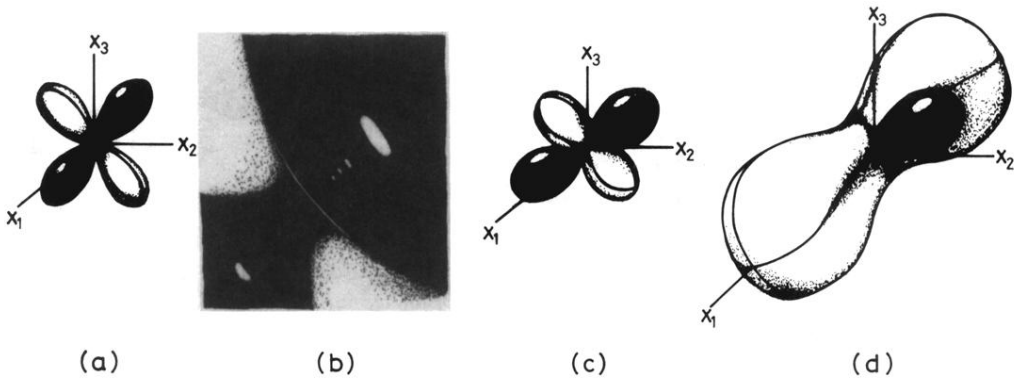

FIG. 38. Schematical representation of the change of the gyration surface of $BaMnF_4$ at various temperatures. (a) 260 K, (b) 253 K($\simeq T_i$), (c) 230 K, and (d) 160 K.